Materials Today Communications 57 (2026) 116616

Contents lists available at ScienceDirect

Materials Today Communications

journal homepage: www.elsevier.com/locate/mtcomm

Hybrid network formation and thermal transport in nanocomposites with dissimilar high-aspect-ratio fillers

Eduard Lysenkov

Petro Mohyla Black Sea National University, 68 Desantnykiv St., 10, Mykolaiv 54003, Ukraine

ARTICLE INFO

Keywords:
Hybrid nanocomposites
Percolation
Effective connectivity
High-aspect-ratio fillers
Thermal conductivity

ABSTRACT

This study develops a generalized analytical model to investigate how inter-filler contacts affect network formation and thermal transport in hybrid nanocomposites containing two dissimilar high-aspect-ratio fillers. The model distinguishes individual filler connectivity from hybrid contacts through a dimensionless contact-efficiency parameter. Applied to a representative carbon nanotube–aramid nanofiber system, the model predicts a nonlinear percolation boundary and shows that, at a carbon nanotube concentration of 0.01, the critical aramid nanofiber concentration decreases from 0.0125 to 0.00556 as the hybrid-contact efficiency increases from 0 to 1. The model also predicts increasing thermal conductivity with increasing total filler concentration and hybrid-contact efficiency. Comparison with an independent analytical model reveals a qualitatively similar concentration-dependent trend, although the predicted magnitudes and curvature differ. These results highlight the role of inter-filler contact efficiency in linking hybrid network formation to macroscopic thermal transport. The proposed mean-field framework provides an analytical basis for investigating hybrid filler systems, while quantitative predictions for specific materials require experimental or numerical parameterization.

1. Introduction

Percolation theory provides a general framework for describing the emergence of long-range connectivity in heterogeneous systems. In composite materials containing dispersed network-forming fillers, the formation of a continuous network is associated with a transition from isolated particles and finite clusters to a system-spanning structure [1]. The corresponding percolation threshold depends on the concentration, geometry, spatial distribution, and mutual arrangement of the network-forming elements [2]. These factors become particularly important for high-aspect-ratio fillers, such as fibers, nanofibers [3], nanowires [4], and nanotubes [5]. Their elongated geometry results in a substantially larger excluded volume compared with approximately equiaxed particles and can therefore strongly affect the concentration required for network formation [6].

High-aspect-ratio fillers are particularly attractive for the formation of functional networks in polymer composites because an interconnected structure can emerge at relatively low filler concentrations [7]. The geometry of such fillers allows individual elements to interact with a large number of neighboring elements and facilitates the formation of extended clusters [8]. Consequently, the aspect ratio is not merely a geometric descriptor of an individual filler but an important parameter governing the collective connectivity of the dispersed phase [9]. At the same time, the formation of a system-spanning network depends not only on the number of potential contacts but also on their spatial organization and their ability to connect otherwise separated clusters [10].

The situation becomes more complex in hybrid composites containing two different types of high-aspect-ratio fillers [11]. In such systems, connectivity may arise from interactions between fillers of the same type as well as from contacts between dissimilar fillers. The resulting network therefore contains three classes of interactions, namely 1–1, 2–2, and 1–2 connections. Their relative contributions depend on the concentrations, aspect ratios, geometrical dimensions, and spatial organization of the two filler populations. In particular, heterotypic contacts can provide additional connections between clusters formed by different filler populations and thereby modify the conditions for the formation of a system-spanning network. Thus, the connectivity of a hybrid high-aspect-ratio network cannot generally be described solely by considering the individual percolation thresholds of its constituent fillers.

An important distinction, however, arises between the formation of a geometrical contact and its contribution to the macroscopic connectivity of a transport network [12]. A network may contain numerous local

E-mail address: ealysenkov@ukr.net.

https://doi.org/10.1016/j.mtcomm.2026.116616
Received 23 September 2026; Received in revised form 26 October 2026; Accepted 7 November 2026
Available online 8 November 2026
2352-4928/© 2026 The Author(s). Published by Elsevier Ltd. This is an open access article under the CC BY-NC-ND license (http://creativecommons.org/licenses/by-nc-nd/4.0/).

contacts without all of them contributing equally to a system-spanning transport pathway. In percolating networks, this distinction is reflected, for example, in the difference between the transport-active backbone and structurally connected branches that do not contribute to the spanning pathway [13]. Consequently, the probability of geometrical contact formation alone does not necessarily provide a complete measure of the functional connectivity of a high-aspect-ratio filler network. This distinction becomes particularly relevant in hybrid systems, where heterotypic contacts may differ from homotypic contacts in their geometry, spatial arrangement, separation distance, and effectiveness for a particular transport mechanism [14].

This consideration suggests that the geometrical probability of forming a heterotypic contact should be distinguished from the contribution of that contact to network connectivity [15]. In the present framework, these two aspects are therefore treated separately. The geometrical contribution characterizes the propensity of two different filler populations to form contacts, whereas an additional efficiency factor is introduced to describe the fraction or effectiveness of such connections that contributes to the functional network. This formulation provides a basis for incorporating the aspect ratios and characteristic dimensions of the fillers [16] as well as the distance-dependent nature of their interaction, without assigning the same physical meaning to every geometrically possible contact [17].

The distinction between geometrical connectivity and transport connectivity is also relevant when the same structural network is considered for different transport mechanisms. For thermal transport, the corresponding contribution may additionally depend on the thermal resistance associated with the interface between neighbouring constituents [18]. Thus, although the geometrical framework for describing network formation can be common to different transport phenomena [19], the efficiency with which individual connections contribute to macroscopic transport need not be universal.

Recent computational studies have explored heat-transfer behavior in nanomaterial-containing systems using a range of mathematical and data-driven approaches. These include numerical analyses of heat transfer in CNT-based nanosystems [20] and hybrid nanosystems [21]. Neural-network-based approaches have also been applied to the prediction of transport behavior in ternary hybrid nanosystems [22]. These works illustrate the broader development of analytical, numerical, and data-driven methods for describing transport in nanomaterial-containing systems.

Previous analytical approaches have also addressed thermal conductivity of hybrid polymer nanocomposites [23,24]. For example, Navidfar and Trabzon developed an analytical model for hybrid polyurethane nanocomposites containing CNT and graphene nanoplatelets, incorporating filler volume fraction, interfacial thermal resistance, nanofiller straightness, and percolation effects [24]. Such approaches demonstrate the feasibility of analytical description of thermal transport in hybrid nanofiller systems, while employing a physical framework different from the connectivity-based formulation considered in the present work.

The objective of this work is to develop a generalized connectivity framework for two-component networks of high-aspect-ratio fillers in which heterotypic interactions are explicitly distinguished from their contribution to network formation. The model is formulated in terms of filler concentration, aspect ratio, geometrical interaction, and network connectivity, and is subsequently extended by considering the efficiency of individual connections. The physical meaning and limiting behavior of the resulting parameters are analyzed, and the framework is demonstrated using a hybrid high-aspect-ratio filler system as a representative model case. Particular attention is given to the relationship between geometrical contacts, network connectivity, percolation, and the resulting transport properties.

2. Mathematical framework for hybrid network connectivity

The theoretical framework developed here builds on the excluded-volume concept introduced by Onsager [25] for anisometric particles and subsequently applied to continuum percolation problems by Balberg and co-workers [26]. This approach provides a physical basis for relating the connectivity and percolation behavior of elongated fillers to their concentration and geometrical characteristics. The present work further develops the connectivity model introduced in our previous study [11], where the contributions of dissimilar high-aspect-ratio fillers and their mutual interactions were incorporated into a unified connectivity parameter.

For a network formed by high-aspect-ratio fillers, the connectivity of a single-component system can be characterized by the aspect ratio of the filler and its volume fraction. For filler i, the aspect ratio is defined as

$$A_i \sim \frac{L_i}{D_i} \tag{1}$$

where L_i and D_i are the characteristic length and diameter, respectively. Within the adopted mean-field description, the corresponding contribution to network connectivity is written as

$$\Psi_i = A_i \varphi_i \tag{2}$$

Thus, the connectivity of a single-component network is proportional to both the filler concentration and its aspect ratio. The higher the aspect ratio, the greater the ability of the filler to contribute to the formation of a connected network. The underlying geometrical considerations are consistent with the approach developed in our previous work.

For a hybrid system containing two types of high-aspect-ratio fillers, the network can be formed through three classes of connections: contacts between particles of type 1, contacts between particles of type 2, and contacts between particles of different types. Accordingly, the effective connectivity parameter is expressed as [11]

$$\Psi_{eff} = A_1\varphi_1 + A_2\varphi_2 + \Gamma\varphi_1\varphi_2 \tag{3}$$

where the first two terms describe the individual contributions of the two filler populations, while the third term represents the additional contribution associated with hybrid contacts. Here, Γ is a coefficient characterizing the contribution of interparticle contacts between different filler types [11].

The hybrid coefficient is further separated into a geometrical and an efficiency contribution:

$$\Gamma = \Gamma_{geom}\eta \tag{4}$$

where Γ_{geom} characterizes the geometrical probability of forming contacts between different filler types, whereas η describes the effectiveness of these contacts in contributing to the continuous transport network. Thus,

$$\Psi_{eff} = A_1\varphi_1 + A_2\varphi_2 + \Gamma_{geom}\eta\varphi_1\varphi_2 \tag{5}$$

In this formulation, η is treated as a dimensionless effective network-activity parameter within the range $0 \le \eta \le 1.0$.

This separation is important because the geometrical existence of a contact does not necessarily imply that the contact contributes effectively to long-range transport.

The three contributions to the effective connectivity can be considered separately as

$$\Psi_{11} = A_1\varphi_1 \quad \Psi_{22} = A_2\varphi_2 \tag{6}$$

and

$$\Psi_{12} = \Gamma_{geom}\eta\varphi_1\varphi_2 \tag{7}$$

Consequently,

$$\Psi_{eff} = \Psi_{11} + \Psi_{22} + \Psi_{12} \tag{8}$$

This representation makes it possible to evaluate separately the contributions of the two single-component networks and the hybrid connections. In particular, the relative importance of hybrid contacts can be characterized by

$$R_{12} = \frac{\Psi_{12}}{\Psi_{11} + \Psi_{22}} \tag{9}$$

while their fraction in the total network connectivity is given by

$$S_{12} = \frac{\Psi_{12}}{\Psi_{eff}} \tag{10}$$

These quantities provide a direct basis for analyzing how the balance between same-type and hybrid contacts changes with filler concentration, aspect ratio, and contact efficiency.

A macroscopic connected network is assumed to form when the effective connectivity reaches a critical value Ψ_c. The percolation condition is therefore written as

$$\Psi_{eff} \geq \Psi_c \tag{11}$$

At the percolation boundary,

$$A_1\varphi_1 + A_2\varphi_2 + \Gamma_{geom}\eta\varphi_1\varphi_2 = \Psi_c \tag{12}$$

For a fixed concentration of the second filler, the critical concentration of the first filler follows as

$$\varphi_{1,c} = \frac{\Psi_c - A_2\varphi_2}{A_1 + \Gamma_{geom}\eta\varphi_2} \tag{13}$$

Similarly,

$$\varphi_{2,c} = \frac{\Psi_c - A_1\varphi_1}{A_2 + \Gamma_{geom}\eta\varphi_1} \tag{14}$$

These expressions show directly how hybrid contacts modify the percolation boundary relative to the case in which the two filler populations contribute independently.

The proposed formulation satisfies several limiting cases that provide a consistency check of the model. When the hybrid contacts do not contribute to network formation, $\eta = 0$, Eq. (3) reduces to

$$\Psi_{eff} = A_1\varphi_1 + A_2\varphi_2 \tag{15}$$

For maximum hybrid-contact efficiency, $\eta = 1$,

$$\Psi_{eff} = A_1\varphi_1 + A_2\varphi_2 + \Gamma_{geom}\varphi_1\varphi_2 \tag{16}$$

Finally, when either filler is absent, the model reduces to the corresponding single-component network:

$$\begin{aligned} \varphi_1 = 0: &\quad \Psi_{eff} = A_2\varphi_2 \\ \varphi_2 = 0: &\quad \Psi_{eff} = A_1\varphi_1 \end{aligned} \tag{17}$$

Thus, the hybrid formulation continuously connects the single-component and two-component limits.

To relate the network connectivity to a macroscopic transport property, a percolation-type scaling relation is adopted [27]:

$$P = C_p\left(\Psi_{eff} - \Psi_c\right)^t \qquad \Psi_{eff} > \Psi_c \tag{18}$$

where P denotes the considered transport property, C_p is a proportionality coefficient, and t is the corresponding critical exponent.

This formulation allows the connectivity model to be applied to different transport phenomena without changing its geometrical core. The transport-specific behavior is introduced through the corresponding prefactor and critical exponent.

For thermal transport [28–30],

$$\lambda = C_\lambda\left(\Psi_{eff} - \Psi_c\right)^k \tag{19}$$

where λ is the thermal conductivity, C_λ is the corresponding scaling coefficient and k is the thermal critical exponent.

3. Application of the model to a representative CNT/ANF hybrid system

To demonstrate the applicability of the proposed connectivity framework, a representative hybrid system containing carbon nanotubes (CNTs) and aramid nanofibers (ANFs) is considered. Both fillers belong to the class of high-aspect-ratio reinforcing elements and can therefore form spatially extended networks at relatively low concentrations. The CNT/ANF system is used here as a model hybrid system rather than as a restriction of the proposed theoretical framework.

For this system, filler 1 is assigned to CNTs and filler 2 to ANFs. The corresponding aspect ratios are defined as

$$A_{CNT} \sim \frac{L_{CNT}}{D_{CNT}};\ A_{ANF} \sim \frac{L_{ANF}}{D_{ANF}}$$

The effective connectivity of the CNT/ANF network is therefore obtained from Eq. (5) as

$$\Psi_{eff} = A_{CNT}\varphi_{CNT} + A_{ANF}\varphi_{ANF} + \Gamma_{geom}\eta\varphi_{CNT}\varphi_{ANF} \tag{20}$$

The first two terms describe the contributions of CNT–CNT and ANF–ANF connections, respectively, whereas the third term represents the additional connectivity associated with CNT–ANF contacts.

The parameters required for the numerical analysis are summarized in Table 1. The geometrical parameters include the characteristic length and diameter of each filler and the resulting aspect ratio. The concentration of each filler is expressed as volume fraction, consistently with the mathematical formulation.

In addition to the geometrical parameters, the model requires the critical connectivity Ψ_c, the geometrical hybrid-contact coefficient Γ_{geom}, and the contact-efficiency parameter η. For thermal conductivity calculations, the scaling coefficient C_λ and the critical exponent k are also required.

The numerical values listed in Table 1 are representative parameters adopted for the model calculations. They are intended to demonstrate the behavior and parameter dependence of the proposed framework rather than to provide a quantitative description of a specific experimentally characterized CNT/ANF composite (Fig. 1).

4. Results and discussion

4.1. Contributions to effective connectivity and role of hybrid-contact efficiency

The formation of the network in a two-filler composite was first analyzed by separating the contributions associated with contacts between similar and dissimilar filler elements. According to the proposed generalized connectivity model, the effective connectivity is expressed as

$$\Psi_{eff} = \Psi_{CNT-CNT} + \Psi_{ANF-ANF} + \Psi_{CNT-ANF}, \tag{22}$$

where $\Psi_{CNT-CNT} = A_{CNT}\varphi_{CNT}$, $\Psi_{ANF-ANF} = A_{ANF}\varphi_{ANF}$ and $\Psi_{CNT-ANF} = \Gamma_{geom}\eta\varphi_{CNT}\varphi_{ANF}$.

For the calculations presented in Fig. 2, equal concentrations of CNT and ANF were considered, with $A_{CNT} = 100$, $A_{ANF} = 80$, $\Gamma_{geom} = 10000$, and $\eta = 1$. The individual-filler contributions therefore increase linearly

Table 1
Representative parameters used in the theoretical analysis of the CNT/ANF hybrid system.

A_{CNT}	A_{ANF}	Ψ_c	Γ_{geom}	η	C_λ	k
100	80	2.0	10000	0–1	1	0.5

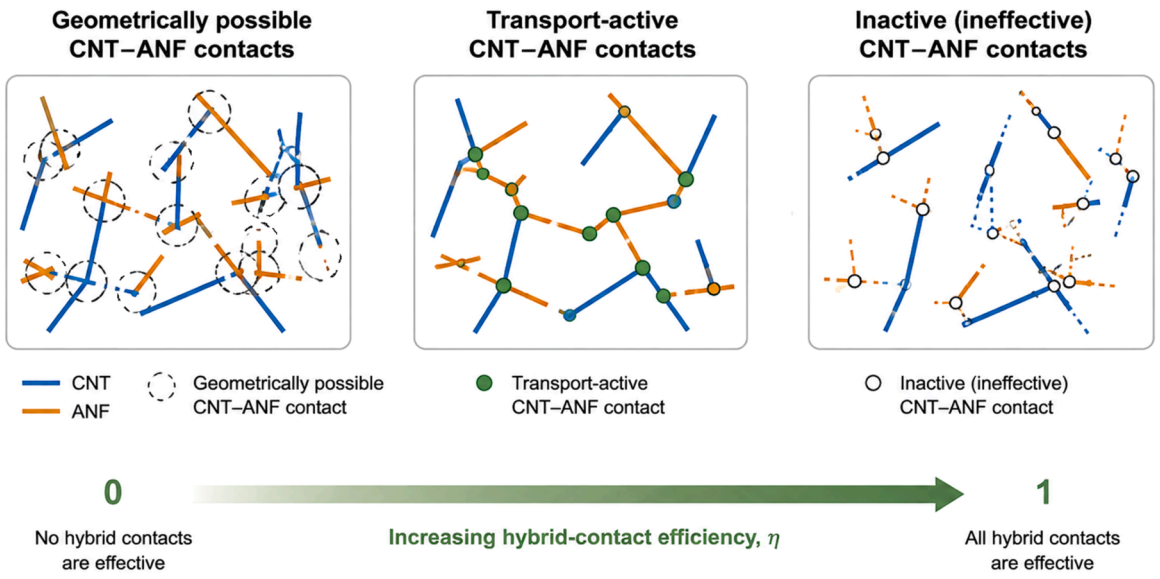


Fig. 1. Schematic interpretation of hybrid-contact efficiency.

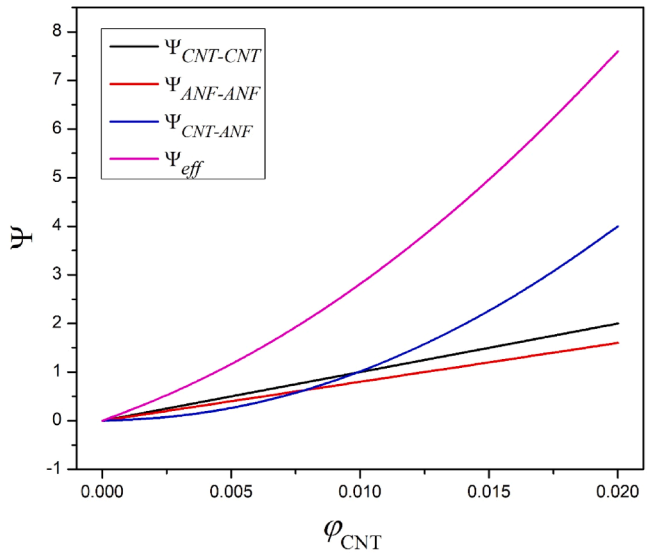


Fig. 2. Contributions of individual and hybrid contacts to the effective connectivity.

with filler concentration, whereas the hybrid contribution increases as the product of the two filler concentrations. This difference in concentration dependence is responsible for the progressively increasing contribution of CNT–ANF contacts to the overall connectivity.

At low filler concentrations, the connectivity is dominated by the individual CNT–CNT and ANF–ANF contributions. For example, at $\varphi_{CNT} = \varphi_{ANF} = 0.002$, these contributions are 0.20 and 0.16, respectively, whereas the hybrid contribution is only 0.04. As the concentration increases, however, the CNT–ANF contribution increases more rapidly than either individual contribution. At $\varphi_{CNT} = \varphi_{ANF} = 0.020$, the corresponding values are 2.0, 1.6, and 4.0, respectively. Thus, under the selected conditions, the hybrid contribution becomes the largest individual contribution to effective connectivity at sufficiently high filler concentration. This behavior is a direct consequence of the bilinear concentration dependence of the hybrid term and does not require assuming a separate percolation mechanism.

The parameter η provides the connection between geometrically possible inter-filler contacts and their contribution to the network (Fig. 1). It is introduced as a dimensionless efficiency parameter satisfying $0 \le \eta \le 1.0$. Physically, it can be interpreted as a fraction of geometrically available CNT–ANF contacts that participate in the transport-relevant network. In an intuitive representation,

$$\eta \approx \frac{N_{active}}{N_{possible}}, \tag{21}$$

where N_{active} denotes the number of inter-filler contacts that contribute to network connectivity and $N_{possible}$ represents the corresponding number of geometrically available contacts. This interpretation should not be regarded as a direct microscopic counting procedure; rather, it provides a physical meaning for the phenomenological parameter η. It distinguishes the existence of a geometrical contact from its effectiveness as a network connection.

This distinction is important for hybrid composites because a geometrically possible contact does not necessarily provide an equivalent contribution to a continuous transport pathway. Some contacts may terminate locally, connect poorly oriented filler segments, or otherwise fail to contribute to long-range network transport. In this respect, the role of η is conceptually analogous to the distinction between active connections and inactive or "dead-end" elements encountered in network descriptions of other heterogeneous materials [31,32]. The analogy is used here only to clarify the physical interpretation of η; the mathematical formulation of the present model remains based on the connectivity and percolation framework.

Fig. 3 further demonstrates the effect of this parameter on the total effective connectivity. For the equal-composition condition $\varphi_{CNT} = \varphi_{ANF}$, the model reduces to $\Psi_{eff} = (A_{CNT} + A_{ANF})\varphi + \Gamma_{geom}\eta\varphi^2$.

When $\eta = 0$, the two filler populations contribute independently and the effective connectivity varies linearly with filler concentration. Increasing η progressively enhances the connectivity through the hybrid CNT–ANF term. Importantly, the effect of η is relatively weak at low concentrations but becomes increasingly pronounced as the concentration increases because the hybrid contribution scales with φ^2.

For example, at $\varphi = 0.002$, increasing η from 0 to 1 changes Ψ_{eff} from 0.36 to 0.40. At $\varphi = 0.010$, the corresponding increase is from 1.80 to 2.80, while at $\varphi = 0.020$, Ψ_{eff} increases from 3.60 to 7.60. Hence, the influence of hybrid-contact efficiency is strongly concentration-dependent. This behavior follows from the multiplicative nature of the hybrid contribution: the effect of improving CNT–ANF contact efficiency can become substantial only when both filler populations are present at sufficient concentration to provide a significant number of potential

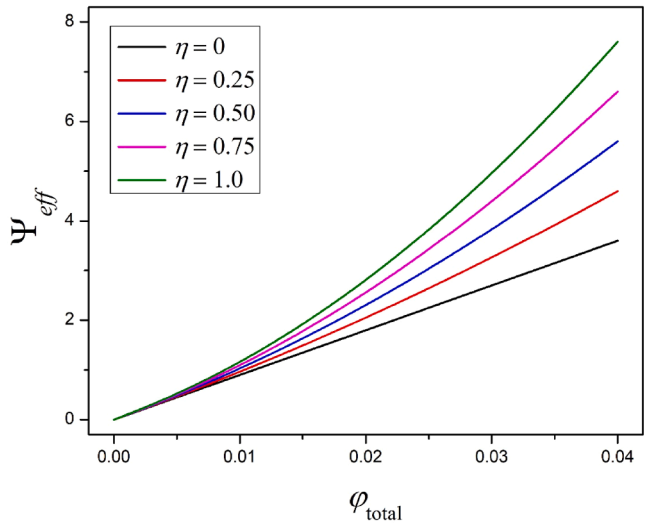


Fig. 3. Effective connectivity as a function of filler composition for different values of η.

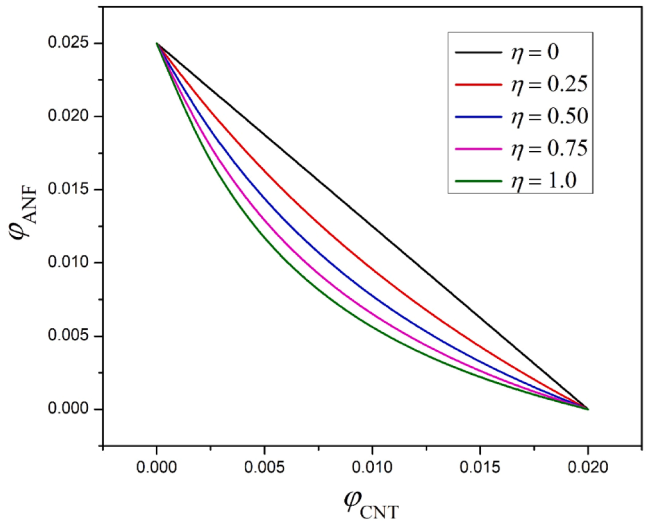


Fig. 4. Percolation boundaries of the CNT/ANF hybrid system for different contact efficiencies.

inter-filler connections.

The results therefore demonstrate that η does not simply act as a scaling factor applied uniformly to the total connectivity. Instead, it selectively controls the hybrid component of the network and consequently determines how strongly the two filler populations cooperate in establishing effective connectivity. The transition from the $\eta = 0$ case, corresponding to two independently contributing filler populations, toward $\eta = 1$, corresponding to the maximum effectiveness considered in the present model, represents an increasing degree of network integration between the two filler types.

The combined results of Figs. 2 and 3 thus provide a physically consistent interpretation of the hybrid term in the generalized connectivity model. The individual contributions describe connectivity generated within each filler population, whereas the cross-term accounts for connectivity arising from interactions between the two populations. The parameter η then distinguishes the geometrical possibility of forming such hybrid contacts from their effectiveness in sustaining the network. Consequently, the model can describe not only the amount of filler present in the composite, but also the degree to which the two filler populations are structurally integrated into a common transport network.

4.2. Effect of hybrid-contact efficiency on the percolation boundary

The effect of the hybrid-contact efficiency parameter η on the percolation behavior of the two-filler system was further examined by constructing the percolation boundary in the $\varphi_{CNT} - \varphi_{ANF}$ composition space (Fig. 4). The boundary corresponds to the critical connectivity condition $\Psi_{eff} = \Psi_c$ and is therefore determined by Ψ_c.

For the parameters used in the present calculations, $A_{CNT} = 100$, $A_{ANF} = 80$, $\Gamma_{geom} = 10000$, and Ψ_c, the corresponding ANF concentration can be expressed as

$$\varphi_{ANF} = \frac{\Psi_c - A_{CNT}\varphi_{CNT}}{A_{ANF} + \Gamma_{geom}\eta\varphi_{CNT}} \tag{23}$$

The resulting curves reveal a pronounced dependence of the percolation boundary on the efficiency of hybrid CNT–ANF connections. In the limiting case of $\eta = 0$, the hybrid contribution vanishes and the connectivity becomes purely additive,

$$\Psi_{eff} = A_{CNT}\varphi_{CNT} + A_{ANF}\varphi_{ANF} \tag{24}$$

Consequently, the percolation boundary is linear in the composition plane. Increasing η introduces the positive cross-term $\Gamma_{geom}\eta\varphi_{CNT}\varphi_{ANF}$, resulting in a progressively nonlinear boundary. Thus, the curvature of the percolation boundary is a direct consequence of the hybrid-contact contribution and provides a graphical representation of the transition from independent filler-network formation toward connectivity assisted by inter-filler contacts.

An important feature of the calculated boundaries is that all curves retain identical intercepts with the coordinate axes. At $\varphi_{CNT} = 0$, the percolation condition is determined exclusively by the ANF–ANF contribution, giving $\varphi_{ANF} = \frac{\Psi_c}{A_{ANF}} = 0.025$. Conversely, at $\varphi_{ANF} = 0$, the condition is determined exclusively by the CNT–CNT contribution and gives $\varphi_{CNT} = \frac{\Psi_c}{A_{CNT}} = 0.020$. The hybrid term cannot contribute at either axis because it is proportional to the product $\varphi_{CNT}\varphi_{ANF}$. Therefore, variation of η does not alter the limiting percolation concentrations of either single-filler system. Its effect is restricted to compositions in which both fillers are simultaneously present.

Within this two-component region, increasing η progressively shifts the percolation boundary toward lower concentrations of both fillers. For example, at $\varphi_{CNT} = 0.010$, the ANF concentration required to reach the critical connectivity decreases from 0.0125 for $\eta = 0$ to 0.00952, 0.00769, 0.00645, and 0.00556 for $\eta = 0.25$, 0.50, 0.75, and 1.0, respectively. Thus, at this composition, complete hybrid-contact effectiveness reduces the ANF concentration required for reaching the percolation condition by more than a factor of two relative to the case of independent filler networks.

This behavior reflects the physical role assigned to η in the model. The parameter does not represent an additional filler concentration or an independent source of connectivity; rather, it determines the fraction or effectiveness of geometrically possible CNT–ANF contacts that contributes to the formation of the transport-relevant network. When $\eta = 0$, the two filler populations contribute independently to the connectivity. As η increases, an increasing fraction of the geometrically available inter-filler contacts becomes effective, providing an additional connectivity contribution that is proportional to $\varphi_{CNT}\varphi_{ANF}$. Because this term depends simultaneously on the concentrations of both components, its influence becomes increasingly pronounced away from the coordinate axes and at higher filler concentrations.

The nonlinear displacement of the boundary therefore has a direct physical interpretation: efficient inter-filler connectivity allows the critical network to be established at compositions for which neither individual filler population, considered independently, would provide sufficient connectivity. In this sense, η controls the degree to which the hybrid architecture departs from a simple superposition of two independent networks. The model consequently predicts that the

composition dependence of the percolation threshold is not determined solely by the aspect-ratio-controlled contributions of the individual fillers, but also by the effectiveness of their mutual connectivity.

It should be emphasized that the present result is a model prediction rather than an assertion that all CNT–ANF systems necessarily exhibit the same quantitative percolation boundaries. The absolute position of the boundaries depends on the selected connectivity coefficients, the geometric interaction parameter, and the critical connectivity value. The robust feature of the calculation is the qualitative transformation from a linear boundary at $\eta = 0$ to a progressively curved boundary with increasing η, together with the preservation of the single-filler intercepts. This behavior follows directly from the mathematical structure of the generalized connectivity model and provides a physically transparent means of quantifying the contribution of hybrid contacts to network formation.

The dependence of the effective connectivity on the CNT content for different values of the CNT aspect-ratio-related connectivity coefficient is shown in Fig. 5. For this analysis, equal CNT and ANF volume fractions were assumed,

$\varphi_{CNT} = \varphi_{ANF}$, while $\Gamma_{geom} = 10000$ and $\eta = 0.5$ were kept constant.

The results demonstrate a pronounced dependence of the effective connectivity on the aspect-ratio-related coefficient of the CNT component. Increasing A_{CNT} from 50 to 1000 substantially increases Ψ_{eff} over the entire investigated concentration range. At $\varphi = 0.010$, for example, Ψ_{eff} increases from 1.8 for $A_{CNT} = 50$ to 11.3 for $A_{CNT} = 1000$. This behavior reflects the direct contribution of the CNT population to network formation: at a given filler concentration, a larger aspect-ratio-related coefficient corresponds to a greater contribution of CNTs to the effective connectivity.

Importantly, the curves exhibit a nonlinear concentration dependence despite the linear dependence of the individual CNT–CNT contribution on φ. This nonlinearity originates from the hybrid CNT–ANF term, which is proportional to $\varphi_{CNT}\varphi_{ANF}$ and therefore becomes proportional to φ^2 under the equal-composition condition. Consequently, the effect of increasing A_{CNT} is superimposed on a concentration-dependent contribution from hybrid CNT–ANF contacts. At higher filler concentrations, this quadratic contribution becomes increasingly significant, resulting in progressively steeper increases in Ψ_{eff}.

The results therefore indicate that filler aspect ratio and hybrid-contact efficiency affect the network connectivity through distinct but coupled mechanisms. The aspect-ratio-related coefficient primarily controls the direct connectivity contribution of the CNT population, whereas the hybrid term introduces an additional concentration-dependent enhancement associated with interactions between the two filler types. Thus, increasing the aspect ratio of one component can substantially modify the connectivity of a hybrid network, particularly when both filler populations are present at appreciable concentrations.

4.3. Thermal transport

The effect of hybrid-contact efficiency on the transport properties predicted by the generalized connectivity model is illustrated in Fig. 6 for thermal conductivity. The thermal transport property was calculated as a power-law function of the excess effective connectivity above the percolation threshold, according to Eq. (19).

A qualitatively similar dependence is obtained for thermal conductivity (Fig. 6). No finite thermal transport contribution is predicted below the connectivity threshold, whereas above the threshold the thermal conductivity increases with both total filler fraction and hybrid-contact efficiency. At $\varphi_{total} = 0.020$, for example, the predicted thermal conductivity increases from zero at $\eta = 0.25$ to 0.50, 0.707, and 0.866 for $\eta = 0.5$, 0.75, and 1, respectively. At $\varphi_{total} = 0.040$, these values increase to 1.60, 1.88, 2.13, and 2.36 for $\eta = 0.25$, 0.5, 0.75, and 1, respectively.

Overall, the results of Fig. 6 establish the connection between hybrid network formation and macroscopic transport within the proposed framework. A higher fraction of transport-active CNT–ANF contacts increases the effective connectivity, facilitates attainment of the percolation condition, and consequently enhances thermal transport. The effect becomes particularly pronounced at higher filler concentrations because the hybrid connectivity contribution increases quadratically with the concentrations of the two filler populations. In this sense, the hybrid-contact efficiency η provides a compact parameter for linking the structural integration of dissimilar high-aspect-ratio fillers with the resulting transport response.

4.4. Comparison with an independent analytical model

To further assess the consistency of the proposed formulation, its predictions were compared with those obtained using the analytical model of Navidfar and Trabzon [24], developed for thermal conductivity of hybrid polymer nanocomposites containing MWCNTs and graphene nanoplatelets. Unlike the present connectivity-based approach, that model accounts for thermal transport through a formulation involving filler volume fraction, interfacial thermal resistance,

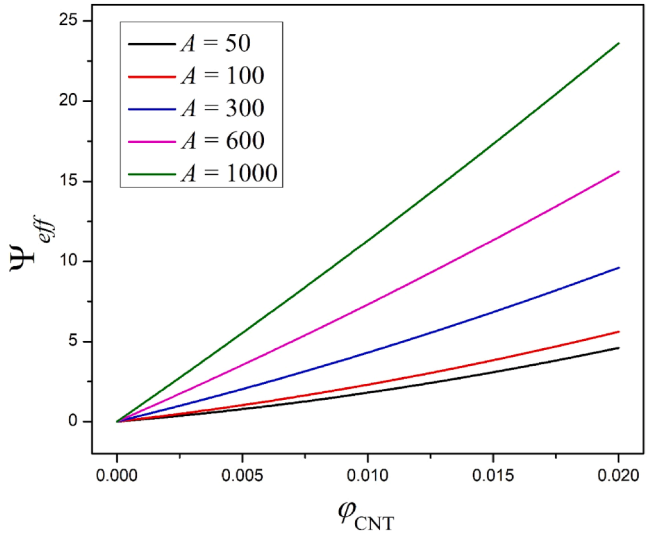


Fig. 5. Effect of CNT aspect ratio on the concentration dependence of effective connectivity.

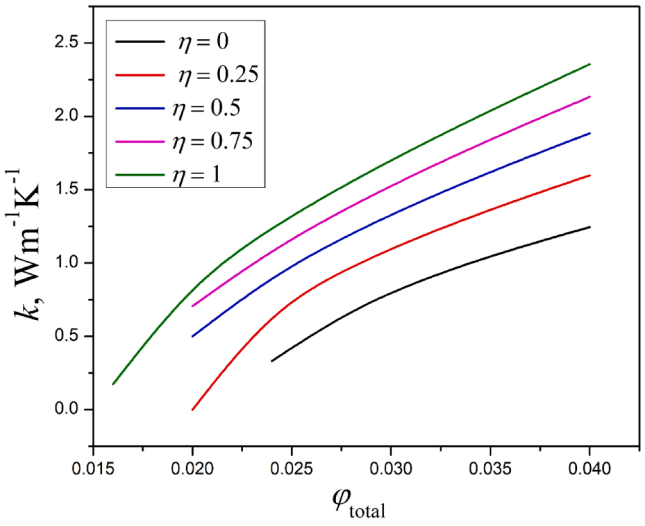


Fig. 6. Predicted thermal conductivity of the CNT/ANF hybrid system for different values of η.

nanofiller straightness, and percolation effects [24]. The comparison was performed for a representative hybrid-filler composition over the same total filler-content range.

As shown in Fig. 7, both analytical approaches predict a nonlinear increase in thermal conductivity with increasing total filler content. Although the absolute values obtained from the two models differ, the predicted concentration dependences exhibit a similar overall shape, with a stronger increase at lower filler contents followed by a progressively weaker rate of increase. This qualitative agreement is noteworthy because the two models are based on different physical formulations: the model of Navidfar and Trabzon incorporates interfacial and geometrical thermal-transport parameters, whereas the present approach describes the thermal response through the connectivity of the hybrid filler network.

The comparison should not be interpreted as a direct validation of either model, since experimental data for the specific CNT/ANF system considered here are not available. Rather, it provides an independent model-to-model consistency check. Despite the differences in the underlying formulations, both approaches predict a nonlinear increase in thermal conductivity with increasing total filler concentration, supporting the physical plausibility of the concentration-dependent response obtained from the proposed connectivity-based formulation.

4.5. Limitations of the model

Despite its ability to describe the effect of filler concentration, aspect-ratio-related connectivity, and hybrid-contact efficiency on the formation of a connected network, the proposed model represents a mean-field description of hybrid filler connectivity and therefore involves several simplifying assumptions. These limitations should be considered when interpreting the quantitative predictions.

First, the model characterizes the contribution of CNT–ANF interactions through the parameter η, which describes the fraction of geometrically available hybrid contacts that contribute to transport-relevant connectivity. This parameter provides a convenient way to account for the fact that not every geometrically possible contact necessarily contributes equally to a macroscopic network. However, η is not derived from an explicit microscopic description of the contact population. In particular, the present formulation does not calculate the spatial distribution, orientation, contact distance, contact area, or local topology of individual CNT–ANF junctions. Consequently, η should be regarded as a structural parameter rather than as a directly measurable microscopic contact fraction.

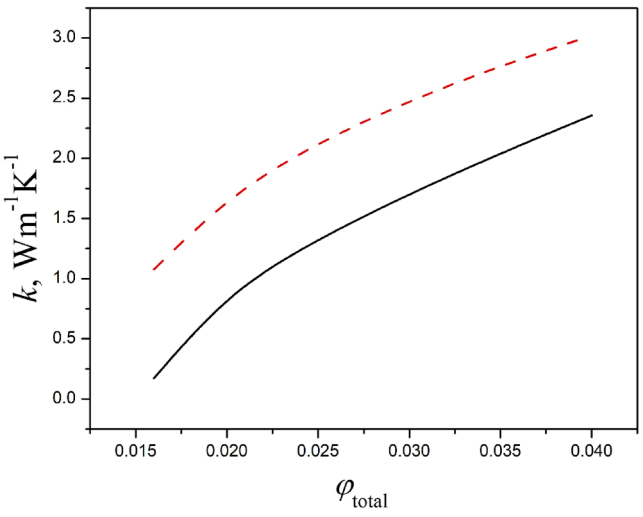


Fig. 7. Comparison of thermal conductivity predictions by the proposed connectivity-based model and the analytical model of Navidfar and Trabzon [24] as a function of total filler concentration.

Second, the model assumes that the connectivity contributions can be represented by the sum of two self-connectivity terms and a hybrid term (Eq. 22). This formulation captures the leading contribution of CNT–CNT, ANF–ANF, and CNT–ANF connections, but it does not explicitly describe spatial correlations between fillers or higher-order structural effects. In real nanocomposites, filler dispersion may involve clustering, orientation correlations, preferential localization, and heterogeneous regions with substantially different local connectivity. Such effects can modify the percolation behavior but are averaged out in the present mean-field treatment.

A further limitation concerns filler aggregation. The model does not explicitly distinguish isolated fillers from aggregated domains or describe how aggregation changes the number and topology of active connections. This is particularly relevant for CNT-based systems, in which aggregation can simultaneously increase local connectivity and reduce the fraction of the filler participating in a sample-spanning network. The parameter η can phenomenologically account for part of this effect, but it does not provide a predictive aggregation model. Therefore, quantitative predictions for a specific material system require η to be determined or constrained using independent structural information.

The transport formulation also represents an idealized description. Thermal properties are calculated from the excess connectivity above the percolation threshold using transport-specific power-law relationships. The thermal formulation does not explicitly include interfacial thermal resistance, phonon scattering, or the intrinsic thermal anisotropy of CNTs and ANFs. Consequently, the predicted transport behavior should be interpreted primarily as the connectivity-controlled component of the response rather than as a complete microscopic description of thermal transport.

Finally, the present analysis uses representative model parameters and systematic parameter variations to demonstrate the behavior of the generalized connectivity framework. The resulting percolation boundaries and transport curves therefore illustrate the consequences of the model assumptions rather than constituting direct predictions for a particular experimentally fabricated composite without parameter calibration. Quantitative application to a specific hybrid nanocomposite requires experimentally or numerically determined values of the connectivity coefficients, critical connectivity, hybrid-contact efficiency, and transport scaling parameters.

These limitations define the intended scope of the model. The proposed framework is not intended to replace detailed microstructural or transport simulations; rather, it provides a compact analytical description of how the concentrations and aspect ratios of two high-aspect-ratio filler populations, together with the efficiency of their mutual connectivity, affect the formation of a hybrid percolating network. More detailed treatment of filler morphology, aggregation, contact topology and interfacial thermal resistance represents a natural direction for further development of the model.

An important limitation of the present study is the absence of experimental validation for the specific CNT/ANF system considered. Although comparison with an independent analytical model provides a useful consistency check, it cannot replace experimental verification. In particular, quantitative assessment of the hybrid-contact efficiency parameter η and the predicted thermal conductivity requires experimental data obtained for well-defined filler geometries, concentrations, dispersion states, and processing conditions.

5. Conclusions

A generalized analytical model for the connectivity of hybrid nanocomposites containing two high-aspect-ratio fillers was developed by separating the contributions of filler–filler and hybrid inter-filler contacts. The effective connectivity parameter includes the individual CNT–CNT and ANF–ANF contributions and an additional CNT–ANF term proportional to the product of the filler concentrations. The hybrid-

contact efficiency parameter η was introduced to account for the participation of geometrically available inter-filler contacts in the transport-relevant network.

Application to the representative CNT/ANF system showed that the hybrid contribution increases quadratically with filler concentration and can become the dominant contribution to effective connectivity at sufficiently high concentrations. Increasing η enhances this contribution and transforms the percolation boundary from a linear relationship into a nonlinear composition-dependent boundary, allowing the percolation condition to be reached at lower concentrations of the individual fillers when both components are present. Increasing the aspect-ratio-related connectivity coefficient of CNTs similarly increases the effective connectivity and strengthens the concentration-dependent network formation.

The predicted thermal transport property exhibits the same fundamental dependence on hybrid connectivity. Increasing the total filler concentration or the efficiency of CNT–ANF contacts increases the excess connectivity above the percolation threshold and consequently enhances thermal conductivity. Comparison with the published analytical model of Navidfar and Trabzon showed a qualitatively similar concentration dependence of the predicted thermal conductivity, while quantitative differences were observed as a consequence of the different model formulations and parameterizations. This comparison provides an analytical benchmark for the proposed connectivity-based approach, although it does not constitute experimental validation.

The model is intentionally formulated as a mean-field description and does not explicitly resolve filler aggregation, orientation, spatial correlations, individual junction characteristics or interfacial thermal resistance. Accordingly, η should be regarded as a structural parameter, and quantitative predictions for specific materials require appropriate experimental or numerical parameterization. Within these limitations, the proposed framework provides a compact analytical basis for describing the connectivity and thermal transport behavior of hybrid systems containing dissimilar high-aspect-ratio fillers.

CRediT authorship contribution statement

Eduard Lysenkov: Writing – original draft, Methodology, Conceptualization.

Declaration of Generative AI and AI-assisted technologies in the manuscript preparation process

During the preparation of this work, the author used ChatGPT-4o (accessed October 2026) for translating certain draft sections to English, as well as for subsequent language editing and grammatical refinement. The author reviewed and edited the output as needed and take full responsibility for the content of the published article.

Declaration of Competing Interest

The authors declare that they have no known competing financial interests or personal relationships that could have appeared to influence the work reported in this paper.

Acknowledgments

This work was funded by the Ministry of Education and Science of Ukraine within the framework of the research project "Creation of multifunctional polymer nanocomposite materials reinforced with para-aramid fibres and carbon nanotubes" (state registration number is 0124U001739).

Data availability

Data will be made available on request.

References

[1] M. Fathidoost, Y. Yang, M. Oechsner, B.X. Xu, Data-driven thermal and percolation analyses of 3D composite structures with interface resistance, Mater. Des. 227 (2023) 111746, https://doi.org/10.1016/j.matdes.2023.111746.
[2] S.K. Sharma, L.K. Sharma, R. Pradhan, Y. Sharma, M. Sharma, S. Gajević, L. Ivanović, B. Stojanović, Interphase-Centric and Mechanism-Driven Advances in Polymer Composites Reinforced with Nano-, Synthetic, and Inorganic Fillers, Polymers 18 (3) (2026) 323, https://doi.org/10.3390/polym18030323.
[3] E.A. Lysenkov, O.V. Striutskyi, V.L. Demchenko, M.M. Lazarenko, The effect of ultra-low concentrations of aramid nanofibers on the structural and thermal characteristics of polylactic acid-based nanocomposites, J. Compos. Mater. 60 (22) (2026) 2071–2077, https://doi.org/10.1177/00219983251399800.
[4] T. Paul, H. Guo, A. Berger, M. Riegler, U. Mansfeld, M. Bianchini, M. Retsch, A. Greiner, Metastable and Electronically Percolating Silver Nanowire–Polymer Composites by Spray Drying, ACS Appl. Mater. Interfaces 18 (7) (2026) 11718–11731, https://doi.org/10.1021/acsami.5c23242.
[5] E. Lysenkov, I. Melnyk, L. Bulavin, V. Klepko, N. Lebovka, Structure of polyglycols doped by nanoparticles with anisotropic shape. Physics of Liquid Matter: Modern Problems, Springer International Publishing, 2015, pp. 165–198, https://doi.org/10.1007/978-3-319-20875-6_7.
[6] M. Khodaei, M. Jafaraghaei, A. Ajrian, S. Giahkar, Review of the percolation threshold for spherocylinder-based systems in a continuum model, Phys. A Statis. Mech. Appl. 680 (2025) 131044, https://doi.org/10.1016/j.physa.2025.131044.
[7] P.K. Vallittu, High-aspect ratio fillers: Fiber-reinforced composites and their anisotropic properties, Dent. Mater. 31 (1) (2015) 1–7, https://doi.org/10.1016/j.dental.2014.07.009.
[8] E.A. Lysenkov, V.V. Klepko, I.P. Lysenkova, Features of microstructure and percolation behavior of polypropylene glycol, filled by multiwalled carbon nanotubes, J. Nano- Electron. Phys. 9 (5) (2017) 05021, https://doi.org/10.21272/jnep.9(5).05021.
[9] J. Qian, J.H. Pu, X.J. Zha, et al., Effect of aspect ratio of multi-wall carbon nanotubes on the dispersion in ethylene-α-octene block copolymer and the properties of the Nanocomposites, J. Polym. Res. 26 (2019) 275, https://doi.org/10.1007/s10965-019-1915-1.
[10] S.U. Kim, J.Y. Kim, Dynamic Statistical Mechanics Modeling of Percolation Networks in Conductive Polymer Composites for Smart Sensor Applications, Materials 18 (13) (2025) 3097, https://doi.org/10.3390/ma18133097.
[11] E. Lysenkov, A theoretical model for double percolation in hybrid polymer nanocomposites reinforced with carbon nanotubes and aramid nanofibers, Nano Express 7 (3) (2026) 035011, https://doi.org/10.1088/2632-959X/ae9bdb.
[12] S.K. Sharma, R. Pradhan, L.K. Sharma, Y. Sharma, Y. Pal, D. Bračun, D. Klobčar, Mechanistic Structure–Property Relationships in Carbon/Polymer Composites: Connectivity, Junction Resistance, and Durability, Polymers 18 (10) (2026) 1220, https://doi.org/10.3390/polym18101220.
[13] B. Gross, I. Bonamassa, S. Havlin, Interdependent transport via percolation backbones in spatial networks, Phys. A Stat. Mech. Appl. 567 (2021) 125644, https://doi.org/10.1016/j.physa.2020.125644.
[14] E. Lysenkov, V. Klepko, L. Bulavin, N. Lebovka, Physico-Chemical Properties of Laponite®/Polyethylene-oxide Based Composites, Chem. Rec. 24 (2) (2024), https://doi.org/10.1002/tcr.202300166.
[15] C. Xu, Y. Zhao, H. Zhang, Morphology-Dependent Percolation and Conductive Network Formation in Polymer Nanocomposites with Multi-Shaped Nanofillers, Nanomaterials 16 (1) (2026) 52, https://doi.org/10.3390/nano16010052.
[16] S. Chen, H. Wang, N. Xu, Transport Percolation Diagram of Composite Medium Predicted by Microscopically Calibrated Lattice Model and Data-Driven Analysis, Appl. Sci. 16 (15) (2026) 7829, https://doi.org/10.3390/app16157829.
[17] K.H. Kim, S.J. Kim, G.Y. Yoo, S.Y. Kim, Advanced percolation models incorporating excluded volume effects in segregated composites via nano-interconnection and micro-void structure optimization, Adv. Compos. Hybrid. Mater. 8 (2025) 452, https://doi.org/10.1007/s42114-025-01520-w.
[18] C. Liu, W. Ma, Y. Lv, et al., Interfaces dominated electrical and thermal percolation properties in nanowire composite, Appl. Phys. A 131 (2025) 565, https://doi.org/10.1007/s00339-025-08687-5.
[19] J. Tan, Y. Zhang, Thermal Conductive Polymer Composites: Recent Progress and Applications, Molecules 29 (15) (2024) 3572, https://doi.org/10.3390/molecules29153572.
[20] R. Baithalu, S.R. Mishra, On optimizing shear rate analysis for the water-based CNT micropolar nanofluids via an elongating surface: response surface methodology combined with ANOVA test, J. Therm. Anal. Calorim. 148 (2023) 14275–14294.
[21] S.R. Mishra, R. Baithalu, S. Ontela, et al., Study of velocity slip impact combined with dissipative heat on the Williamson hybrid nanofluids with the Cattaneo–Christov heat flux framework, J. Therm. Anal. Calorim. 149 (2024) 15305–15322, https://doi.org/10.1007/s10973-024-13769-2.
[22] G.K. Ramesh, R. Saadeh, J.K. Madhukesh, A. Qazza, U. Khan, A. Zaib, et al., Neural network algorithms of a curved riga sensor in a ternary hybrid nanofluid with chemical reaction and Arrhenius kinetics, J. Radiat. Res. Appl. Sci. 17 (4) (2024) 101078, https://doi.org/10.1016/j.jrras.2024.101078.
[23] A. Agrawal, A. Satapathy, Mathematical model for evaluating effective thermal conductivity of polymer composites with hybrid fillers, Int. J. Therm. Sci. 89 (2015) 203–209, https://doi.org/10.1016/j.ijthermalsci.2014.11.006.
[24] A. Navidfar, L. Trabzon, Analytical modeling and experimentally optimizing synergistic effect on thermal conductivity enhancement of polyurethane nanocomposites with hybrid carbon nanofillers, Polym. Compos. 42 (2021) 944–954, https://doi.org/10.1002/pc.25877.

[25] L. Onsager, The Effects of Shape on The Interaction of Colloidal Particles, Ann. New. Y. Acad. Sci. 51 (4) (1949) 627–659, https://doi.org/10.1111/j.1749-6632.1949.tb27296.x.
[26] I. Balberg, C.H. Anderson, S. Alexander, N. Wagner, Excluded volume and its relation to the onset of percolation, Phys. Rev. B 30 (1984) 3933–3943, https://doi.org/10.1103/PhysRevB.30.3933.
[27] D. Stauffer, M. Sahimi, Scaling Theory of Percolation Clusters, in: R.A. Meyers (Ed.), Encyclopedia of Complexity and Systems Science, Springer Berlin Heidelberg, 2020, pp. 1–12, https://doi.org/10.1007/978-3-642-27737-5_464-2.
[28] K. Sun, Z.D. Zhang, L. Qian, F. Dang, X.H. Zhang, R.H. Fan, Dual percolation behaviors of electrical and thermal conductivity in metal-ceramic composites, Appl. Phys. Lett. 108 (6) (2016) 061903, https://doi.org/10.1063/1.4941758.
[29] E.A. Lysenkov, R.V. Dinzhos, Theoretical analysis of thermal conductivity of polymer systems filled with carbon nanotubes, J. Nano- Electron. Phys. 11 (4) (2019) 04004, https://doi.org/10.21272/jnep.11(4).04004.
[30] E.A. Lysenkov, Z.O. Gagolkina, E.V. Lobko, Y.V. Yakovlev, S.D. Nesin, V.V. Klepko, Structure-property relationships in polymer nanocomposites based on cross-linked polyurethanes and carbon nanotubes, Funct. Mater. 22 (3) (2015) 342–349, https://doi.org/10.15407/fm22.03.342.
[31] S.P. Rigby, The Role of Pore Network Structure in the Performance of Heterogeneous Catalysts, Surfaces 9 (2) (2026) 54, https://doi.org/10.3390/surfaces9020054.
[32] G. Amit, D. Ben Porath, S.V. Buldyrev, A. Bashan, Percolation in fractal spatial networks with long-range interactions, Phys. Rev. Res. 5 (2023) 023129, https://doi.org/10.1103/PhysRevResearch.5.023129.